Vibronic dynamics of I_2 trapped in amorphous ice: Coherent following of cage relaxation

V. Senekerimyan, I. Goldschleger, and V. A. Apkarian[a)]
Department of Chemistry, University of California, Irvine, California 92697-2025, USA

(Received 10 September 2007; accepted 8 October 2007; published online 7 December 2007)

Four-wave mixing measurements are carried out on I_2-doped ice, prepared by quench condensing the premixed vapor at 128 K. Coherent vibrational dynamics is observed in two distinct ensembles. The first is ascribed to trapping in asymmetric polar cages in which, as in water, the valence absorption of the molecule is blueshifted by 3500 cm^{-1}, predissociation of the *B* state is complete upon the first extension of the molecular bond, and the vibrational frequency in the ground state (observed through coherent anti-Stokes Raman scattering) is reduced by 6.5%. The effect is ascribed to polarization of the molecule. The implied local field and the ionicity of the molecule are extracted, to conclude that the molecule is oxygen bonded to one water molecule on one side and hydrogen bonded on the other side. The second ensemble is characterized by the transient grating signal, which shows coherent vibrational dynamics on the *B* state. The small predissociation rate in this site suggests a symmetric cage in which the local electric field undergoes effective cancellation; and consistent with this, the extracted blueshift of the valence transition in this site ($\sim$1500 cm^{-1}) coincides with that observed in clathrate hydrates of iodine. Remarkably, in this site, the vibrational period of the *B* state packet coherently stretches from an initial value of 245 fs to 325 fs in the course of five oscillations (1.3 ps), indicative of vibrationally adiabatic following of the cage expansion. The dynamics is characteristic of a molecule trapped in a tight symmetric cage, with a soft cage coordinate that relaxes without eliciting elastic response. Enclathration in low-density amorphous ice is concluded. © *2007 American Institute of Physics*. [DOI: 10.1063/1.2803922]

INTRODUCTION

We employ molecular halogens as reporters of local structure and dynamics to investigate their various hydrated environments with particular interest in developing spectroscopic probes of clathrate hydrates. The ultraviolet-visible (UV-Vis) absorption spectra of halogens undergo distinct blueshift and broadening when hydrated, as already reported for bromine[1,2] and iodine.[3] The shift is associated primarily with the extent of oxygen bonding. The 1:1 $H_2O:X_2$ complex is oxygen bonded, with the lone-pair electrons of oxygen overlapping the empty σ^* orbital on the halogen.[4–6] Since the visible absorption spectra of halogens consist of $\sigma^* \leftarrow \pi^*$ transitions, they undergo a blueshift due to the bound-repulsive interaction along the H_2O-X_2 coordinate—a shift that can be regarded as a marker for the extent of oxygen bonding in the ground electronic state. While in water and amorphous ice the spectra are dramatically shifted, in the clathrates, where all oxygen atoms of the lattice are fully hydrogen bonded, smaller blueshift characteristic of the various clathrate structures is observed.[2,3] The vibrational frequency of the halogen molecule is another marker of the local structure, as was recently demonstrated in the identification of polymorphs of bromine clathrate hydrates.[7] This may be most directly related to the ionicity of the hydrated halogen bond. Electronic structure calculations on $H_2O:Br_2$ and $H_2O:Cl_2$ complexes show that, although there is no intermolecular charge transfer, the molecular halogen is strongly polarized: $H_2O:X^{\delta+}X^{\delta-}$, with a partial charge $\delta \sim 0.04-0.05$.[4–6] The extent of polarization of the molecule will be controlled by the local electric field, which in turn can be expected to be directly correlated with the vibrational frequency of the probe molecule, as amply demonstrated in simulations of water.[8] These spectroscopic markers of local structure are reinforced in the present investigations of iodine doped in amorphous ice. Our principal aim is the characterization of cage dynamics through time-resolved measurements.

Time-resolved measurements of hydrated bromine have proven rather informative.[1,9] In what is spectroscopically characterized as Br_2-doped amorphous ice, we observe a subensemble of molecules that evolve quantum coherently on the electronically excited *B* state of the molecule. The vibrational coherence of the molecule was imaged through the $Br_2^-H_2O^+$ charge transfer state, taking advantage of the sharp nature of this transition. The insulation of the molecule from the dielectric disorder of ice and the decoupling of its vibrational dynamics from the rest of the solid are taken as demonstrations of enclathration—trapping in highly symmetric cages that are assembled by the molecule in the ice. This is consistent with the findings that air trapped in ice sheets and ice cores impresses the clathrate structure locally.[10] Iodine is known to not make clathrate structures directly, but can be induced to occupy clathrate cages when assisted by a

[a)]Electronic mail: aapkaria@uci.edu

help molecule such as tetra hydro furan (THF).[3] It would then be useful to interrogate what distinguishes the local iodine-ice interactions—a query that we address in the present study through time-resolved four-wave mixing spectroscopy. Indeed, the measurements reveal that I_2 can be found in a variety of sites in the amorphous solid, including self-imposed clathrate-type structures. Most remarkably, in such sites, we observe coherent vibrational dynamics that undergoes period elongation, which we interpret as coherent following of the cage coordinate as it relaxes.

Vibronic dynamics of caged dihalogens has been extensively studied in rare gas matrices.[11–13] Cage motion can be directly seen when the molecule is prepared on dissociative molecular potentials, which are strictly cage bound.[14] Alternatively, cage dynamics in the form of zone-boundary phonons can be seen when the probe transition is modulated by the motion.[14–16] Where the molecular spring constant is significantly larger than the characteristic frequencies of the lattice phonons, the molecular vibrational coherence undergoes period compression due to vibrational relaxation in the anharmonic molecular potential. The period compression, under the assumption of linear anharmonicity (Morse potential) is the principal source of characterization of vibrational dissipation rates.[17] The signature of cage dilation has been observed as a faint elongation (~5% elongation after ~15 cycles of motion) of the molecular vibrational period when I_2 is prepared near the bottom of the B state in solid Ar, in a region where the vibrational relaxation rate of the molecule is small.[15] In the present, for I_2 enclathrated in ice, we see a dramatically larger effect of cage accommodation: we observe the vibrational period of the molecule to stretch from 245 to 325 fs in the course of five oscillations (1.3 ps), without loss of vibrational coherence. This rather unusual cage dynamics—the opening of a soft cage mode in slow enough motion to allow the molecule to follow with full retention of vibrational coherence—presumably reflects the very local nature of the cage, which is supported by a bulk of low-density amorphous ice.

EXPERIMENT

The samples are prepared by vapor deposition of the premixed vapor in the ratio 1:1000 of I_2:H_2O, on a 500-μm-thick sapphire substrate held at 128 K. A second bulb containing pure water vapor is used to cover the sample, to ensure that I_2 does not leach under vacuum. Sample thicknesses used was on the order of 200 μm. Measurements were conducted at the deposition temperature of 128 K, both before and after annealing at 155 K. The experimental setup used in these measurements has been described in detail elsewhere.[1] Briefly, the laser system consists of a Ti:sapphire oscillator operating at 790 nm. The output is amplified regeneratively to deliver 0.6 mJ pulses at 1 kHz and is split in 70/30 ratio, with the stronger arm used to pump an optical parametric amplifier (OPA) to generate tunable visible pulses. The leftover is used for second harmonic generation in a 200 μm beta barium borate (BBO) crystal. The OPA output is compressed down to 60 fs using a pair of SF10 prisms. The pulse elongation of the second harmonic at 395 nm is precompensated using a pair of quartz prisms. The experimental time resolution is 90 fs, as measured by four-wave mixing on a 500 μm sapphire substrate in the same geometry of the experiments.

The four-wave mixing (FWM) measurements are carried out using three noncollinear beams in the boxcar geometry, using a single (f=15 cm) achromatic lens to focus onto the sample. Two coincident visible beams are used to write the optical grating, and the second harmonic is used to read the grating along $\mathbf{k}_4=\mathbf{k}_1-\mathbf{k}_2+\mathbf{k}_3$. Since $\lambda_1=\lambda_2$, the detected radiation is at $\lambda_4=\lambda_3$, i.e., at the same color as the probe laser. The FWM under this phase matching condition contains contributions from transient grating (TG) and coherent anti-Stokes Raman scattering (CARS) on the electronically excited and ground states, respectively. A monochromator coupled to a photomultiplier tube is used for spectrally integrated detection. Improvement of the signal-to-noise ratio is obtained by synchronously chopping one of the visible beams at 500 Hz, using a phase-locked loop referenced to the Pockels cell of the regenerative amplifier. The signal is then collected with a boxcar integrator operating in toggle mode (alternating polarity of the input amplifier) and averaged for 1000 pulses. Frequency resolved measurements are conducted using a monochromator coupled to a charge coupled device camera. Measurements were carried out on gratings prepared at $\lambda_1=\lambda_2$=512, 493, and 550 nm, always probed at λ_3=395 nm. In the data reported here, all three input beams have the same polarization.

RESULTS AND ANALYSIS

The absorption spectra of gaseous iodine, iodine in clathrate-hydrates, in water, and in ice are shown in Fig. 1. The absorption, which is dominated by the $B(^3\Pi_u) \leftarrow X(^1\Sigma_g^+)$ electronic transition, peaks at 450 nm in water and in ice, and at 490 nm in the clathrate. The spectra are blue-shifted by 3500 cm^{-1} in the former, and by 1500 cm^{-1} in the latter. Note, I_2 does not form a clathrate on its own. It is prepared as a mixed hydrate, with THF or CH_2Cl_2 as the main guest and iodine as a minority component, which occupies $5^{12}6^4$ cages.[3] While I_2 isolated in rare gas solids fluoresces over a variety of transitions,[18,19] attempts at observing fluorescence in hydrated iodine failed.

The measurements in ice reveal significant sample inhomogeniety. The FWM signal intensity and the observed dynamics vary from spot to spot on the same sample, with spot size determined by the beam waist of the laser of 50 μm. In certain spots, sharp coherent oscillations are observed, suggesting the existence of ordered domains. Two distinct behaviors are identifiable when pumped at 512 nm and probed at 395 nm: (1) oscillatory signal with B-state periods and (2) oscillatory signal with X-state periods, along with regions in which both signals coexist. Note, the Bragg-diffracted signal along $\mathbf{k}_4=\mathbf{k}_1-\mathbf{k}_2+\mathbf{k}_3$ allows the observation of B-state dynamics through resonant TG when the pump excitation is resonant with the $B \leftarrow X$ transition,[1] or X-state vibrational dynamics through CARS, when the pump excitation is preresonant with the $B \leftarrow X$ transition, as extensively reported in

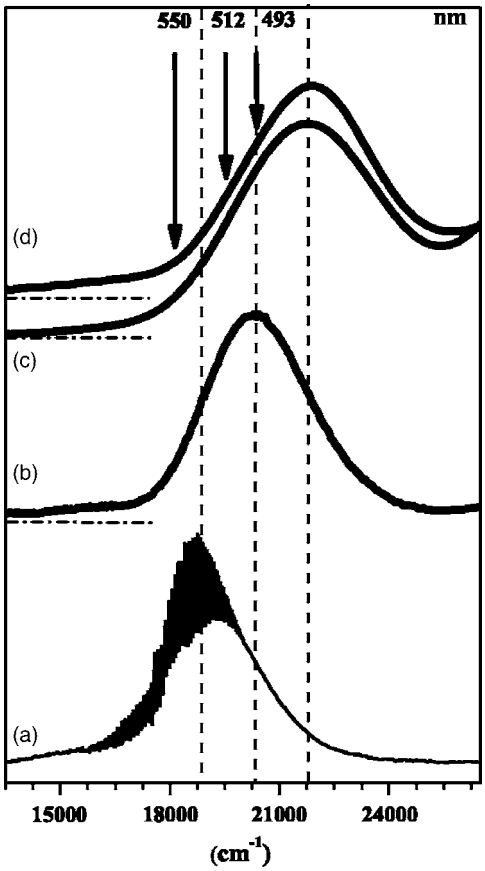

FIG. 1. Absorption spectra: (a) I_2 in gas phase at 295 K, (b) I_2/THF clathrate hydrate at 273 K (Ref. 3), (c) aqueous solution of I_2 at 273 K, (d) I_2 in amorphous ice at 128 K. Dash-dot horizontal lines show the base line in each measurement. The arrows show the excitation wavelengths used in the FWM measurements.

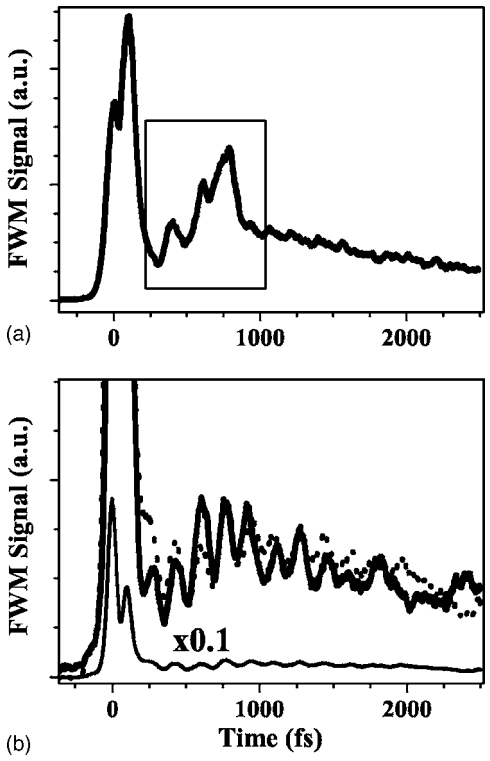

FIG. 2. FWM signal of I_2 in ice: (a) at the deposition temperature of 128 K, before annealing, and (b) signals recorded at annealing temperature of 155 K (solid line), and at 128 K after annealing (dotted line). The observed oscillations are due to the vibrational coherence on the ground X state. In both cases, a peak is observed at 100 fs, with amplitude eight times higher than subsequent oscillations (after multiplying the signal by 0.1; solid black line).

I_2-doped rare gas solids.[20–22] The observation of one or other of these signals with the same pump and probe lasers but in different spots of the solid clearly reflects site inhomogeniety and the dramatic site induced shift in the $B \leftarrow X$ resonance. It can be seen from Fig. 1 that 512 nm excitation corresponds to the peak of the $B \leftarrow X$ absorption in the clathrate structure and to the tail of the band in ice. Indeed, the observed X-state dynamics betrays a strongly polarized molecule, consistent with trapping in frozen water; while the observed B-state dynamics selects an ensemble of molecules that is isolated in an immediate cage structure that is clathratelike. We should note that the observed signal intensities from the different ensembles are comparable in magnitude, suggesting that the strengths of transitions involved in the pump and probe resonances are comparable.

X-state dynamics

In the present experimental scheme, the two coincident beams that prepare the grating at a given color have sufficient bandwidth to create vibrational superposition on the ground electronic state. Thus, for degenerate excitation at $\lambda_{pump}=\lambda_{Stokes}=512$ nm, vibrational states within the convolution width of the laser, $\sqrt{2}\Delta\omega_{laser}=350\ cm^{-1}$, can be prepared coherently. Given the gas phase harmonic frequency $\omega_e=214.5\ cm^{-1}$ and anharmonicity $\omega_e x_e=0.614\ cm^{-1}$ of $I_2(X)$,[23,24] coherent preparation of principally the $|v=0\rangle+|v=1\rangle$ superposition is to be expected. The CARS signal arises from the scattering of the probe beam on the vibrational coherence (phase grating), while the transient grating signal arises from the population (amplitude grating) prepared on various electronic surfaces. The two contributions appear in the signals of Figs. 2 and 3, as the oscillatory CARS signal riding over the TG signal from the incoherent population

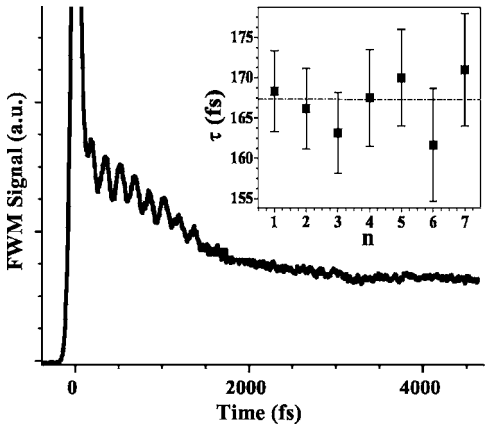

FIG. 3. FWM signal in I_2 enclathrated in ice. Measurement in a sample prepared under similar conditions as in Fig. 2, recorded at 155 K. The insert shows the period of oscillations obtained from six measurements carried out in three different samples (excitation wavelength is 512 nm). The dashed horizontal line shows the average period of 167 fs.

background. The measurement shown in Fig. 2(a) is recorded at the deposition temperature of 128 K, before annealing the sample; the two measurements shown in Fig. 2(b) are at the annealing temperature of 155 K and postannealing at 128 K. The preannealed sample is subject to structural instability that leads to light scattering events, an example of which is captured in the trace in Fig. 2(a) (shaded area). Quench condensation of water below 130 K is known to result in the formation of predominantly low-density amorphous ice,[25,26] and annealing at 155 K is known to lead to crystallization into cubic ice (I_c).[27,28] The intensity jump in the preannealed sample, which must be associated with the motion of micrometer-size grains, takes place on the time scale of 1 min (the scan time of the entire trace is 4 min). The effect is suggestive of sintering or Ostwald ripening,[29,30] which can occur if defects have significant mobility. At 128 K, while defects in ice are locked, a glass transition is known to connect the low-density amorphous phase to the frozen "water *B*" phase.[27] It is quite likely that such a transition can be triggered photothermally during laser irradiation. What is clear is that structural change on macroscopic scales occurs during the measurements in preannealed samples. Once annealed, lowering the temperature back to 128 K eliminates the instability. The signals shown in Figs. 2 and 3 contain a response limited coherence peak, which arises from both resonant and nonresonant contributions. This is followed by the oscillatory part that rides over an incoherent background. The amplitude of the first recursion peak observed at 100 fs [Fig. 2(b)] is eight times stronger than subsequent oscillations. This appearance time of this peak is 15% longer than the half-period of subsequent oscillations and must arise from the predissociative *B* state (see below). Despite the variation of the incoherent background, a meaningful analysis of the oscillations is possible. To be systematic, the signal is fitted as a multi-Gaussian to extract the position, amplitude, and width of the peaks. The insert in Fig. 3 shows the average periods of oscillations obtained from six measurements, performed in three different samples that were prepared under similar conditions. The error bars shown are for the set; otherwise the uncertainty in determining peak positions is approximately ±7 fs. The average period extracted from all six measurements is 167±3 fs, and does not show a measurable variation with time. The oscillations decay with a time constant of ~1.2 ps, independent of annealing history. It is reasonable to assign the observed coherence to the $|0\rangle + |1\rangle$ superposition, in which case the period of 167 fs would translate into a level spacing of $\omega_{10}=199.6\ \mathrm{cm}^{-1}$, which is 6.4% shorter than that of the free molecule: $\omega_{10}=\omega_e - 2\omega_e x_e = 213.27\ \mathrm{cm}^{-1}$. This is a significant reduction in the molecular spring constant, larger than what is observed for iodine dissolved in strongly interacting liquids, such as dioxane.[31,32] In contrast, the vibrational frequency of iodine in the clathrate hydrate is nearly identical to that of the free molecule. In the series of studied solvents by Kiefer, the spectral blueshift of the visible absorption band and the reduction in the vibrational frequency are directly correlated—they take a jump between polar (multipolar) and nonpolar solvents. Rather than intermolecular charge transfer, the significant weakening of the molecular bond can be associated with electrostatics, as recognized by the far IR measurements.[33] This is directly confirmed in the present system. In the ice structure, where the absorption band is shifted by 3500 cm^{-1}, we observe a very large softening of the molecular bond; in contrast, in the symmetric clathrate cages where the blueshift is less than half as large, the spring constant of the molecule is essentially unperturbed.[3] The effect can be directly related to the polarization of the molecule by the local electric field.

Let us estimate the implied ionicity of the observed molecule and the required electric field to induce such a polarization. Thus, if we were to ascribe the softening of the molecular bond entirely to the admixture of ion-pair character in the ground electronic state, then for an electronic wavefunction given as $\psi=\alpha\phi(I_2)+\beta\phi(I^+I^-)$, the potential energy of the mixed state may be constructed as $V=\alpha^2V(I_2)+\beta^2V(I^+I^-)$, where $\alpha^2+\beta^2=1$. This is in the spirit of diatomics in ionic systems, which has been successfully applied to analyze vibrational redshifts[34] and to reproduce details of potential energy surfaces for molecular halogens[35] and hydrogen bonding in HF (Refs. 36 and 37) and H_2O.[38] The lowest ion-pair state which is dipole coupled to the ground is the $D(0_u^+)$ state.[39] We note that in the free molecule, the ion-pair states are split by exchange energy, which would be absent in the broken symmetry of a strong field. As such, for $V(I^+I^-)$ we use the mean of the exchange split pair, $[V(D(0_u^+))+V(E(0_g^+))]/2$. Using the known Morse parameters for the ion pairs and the ground *X* state, we vary the ionic admixture and solve for the vibrational eigenvalues. A bond ionicity of $\beta^2=0.05$ reproduces the observed value of $\omega_{10}=200\ \mathrm{cm}^{-1}$. This value is consistent with what is obtained in *ab initio* treatments of $H_2O:Br_2$ and $H_2O:Cl_2$ complexes.[4,6] Besides softening, 5% ionicity stretches the bond from its equilibrium value of $r_e=2.66$ Å to $r_e'=2.7$ Å, and implies an induced dipole of $\mu_I=0.65$ D. Assuming this to be induced by the permanent dipole of a water molecule ($\mu_p=1.8$ D), the required H_2O-I_2 separation can be calculated as $l=(2\alpha\mu_p/\mu_I)^{1/3}=3.85$ Å, in which $\alpha=10.34\ \text{Å}^3$ is the polarizability of iodine. This is too short in comparison to what would be expected based on the van der Waals contact separation of ~4.8 Å. Were we to assume I_2 to be sandwiched between a pair of water molecules, with their dipoles aligned such that I_2 is O bonded on one end and H bonded on the opposite end, as in the motif seen in small clusters,[40] then the required separation would be $l=4.85$ Å—a rather reasonable value? It is safe to conclude that the molecules observed on the *X* state are trapped in asymmetric, polar cages. It is also safe to conclude that, both in water and in amorphous ice, I_2 is strongly polarized by oxygen bonding to one water molecule and hydrogen bonding to another (along its molecular axis).

B-state dynamics

The *B*-state dynamics is followed in the preannealed samples, in what is expected to be the low-density amorphous ice. In regions where the *B*-state signal is observed exclusively, the solid is not subject to the instabilities noted above. The TG signals obtained for populations prepared at

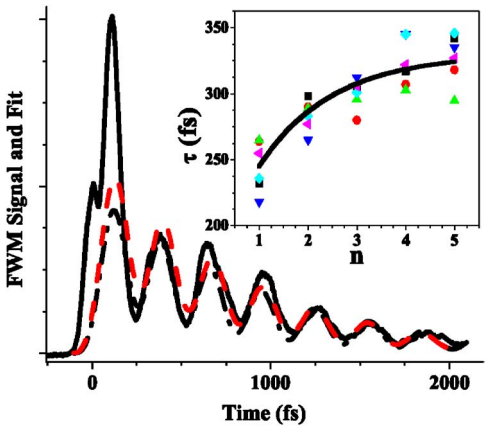

FIG. 4. (Color online) FWM signal of I_2 enclathrated in ice. (a) TG signal at 512 nm excitation (solid line) and fit using Eq. (2) in the text (dash-dot line), simulation signal according to the cage following model discussed in text (dashed line). The change in the period of oscillations for six measurements in two different samples along with the fit to the average of all the six measurements is shown on the insert.

512 and 493 nm while probed at $\lambda=395$ nm are shown in Figs. 4 and 5, respectively. Measurements were also attempted at a pump wavelength of 550 nm, but no signal could be observed. At $t=0$, a response limited peak saturates the signal. While at 512 nm (Fig. 4), fully modulated, damped oscillations are observed for five to six periods; at 493 nm, a single peak delayed by 300 fs is observed (Fig. 5). In both cases, the observed signal can be uniquely assigned to arise from the B state. The absorption spectra in Fig. 1 make it clear that the cross section for exciting into the B state is larger at 493 nm than at 512 nm, therefore the preparation of a population grating is unavoidable. The disappearance of the signal after the first large amplitude excursion of the molecular bond (half-period of 300 fs) must be ascribed to complete predissociation when the molecule is prepared at 493 nm (above the dissociation limit of the free molecule). This is not too surprising, since the B state of I_2 is subject to solvent induced predissociation,[41] and the effect can be expected to be larger in polar solvents since dipolar coupling is the leading term in determining the electronic mixing in the main predissociation channel—the crossing between the $B(^3\Pi_u)$ and the $a(1_g)$ surfaces.[42] Evidently, when prepared at

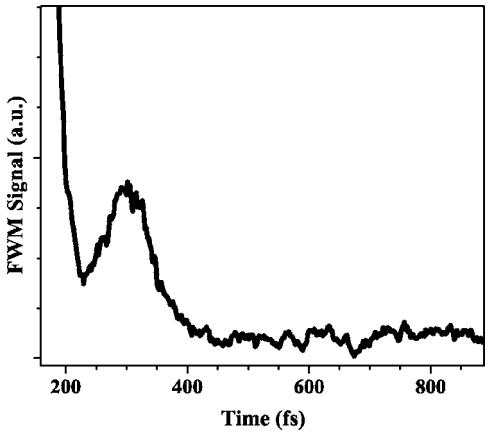

FIG. 5. TG signal obtained with 493 nm excitation. A single recursion is observed at $t=300$ fs.

512 nm, a significant fraction of the population remains trapped on the B state. Based on the ratio of the intensity in the first recursion and second recursion, we can estimate that of the population promoted to the B state, ~50% undergoes curve crossing in the first bond extension. The population that survives undergoes coherent vibrational motion and leaks out on the time scale of 1 ps (see below). This leakage rate is nearly five times smaller than in simple liquids, such as CCl_4,[43,44] and a factor of 2 larger than what is observed in cryogenic Kr matrices.[44] The large survival probability of the population in the present, in cages constructed of water molecules, is only possible if the cage were highly symmetric such that dipolar coupling among electronic states is effectively cancelled—electronic caging by symmetry.[44] As we expand below, energetics, dynamics, and spectroscopy of this ensemble identify it to be in clathrate-type cages.

The rather remarkable feature of the vibrational coherence observed at 512 nm is that the period of motion stretches with time. The insert to Fig. 4 shows the observed recursion times as a function of recursion number obtained from six measurements, and recorded in two different samples prepared under similar conditions. The trend of period elongation is similar in all six measurements, even though the values show a spread that is outside measurement error. Through a multi-Gaussian fit of the data, peak positions are determined with a precision of ±6 fs; however, the spread in oscillation periods may be as large as 40 fs (Fig. 4, insert). We attribute the observed dispersion to the inhomogeneity of the distribution of trap sites. Two related effects may contribute to the dispersion in vibrational periods: the spread in the spectral shift of the $B \leftarrow X$ transition, which controls the prepared initial vibrational energy; and the local cage potential that may modify the spring constant of the trapped molecule. In all cases, the time dependence of the period elongation (chirp) is similar. The mean chirp for the full data set can be represented by an exponential,

$$\tau(t) = \tau_0 + \Delta\tau(1 - e^{-\alpha t}), \tag{1}$$

with initial period of $\tau_0=245$ fs, amplitude $\Delta\tau=80$ fs, and chirp rate $\alpha=0.83$ ps^{-1}. The observed final period, after six cycles, has a mean value $\tau(\infty)=325$ fs. Contrary to a vibrational packet evolving in an anharmonic potential where relaxation would lead to period contraction, we see a dramatic period elongation. The observed period elongation would imply a time dependent reduction in the effective spring constant in the B state of $(\tau_1/\tau_2)^2=k_2/k_1=0.53$. We ascribe the effect to relaxation of the confining cage, and note that the molecular vibrations seem to follow this slow coordinate with retention of coherence.

To characterize the extent of coherence during the motion, we fit the signal to the form of a Gaussian packet detected under a stationary Gaussian window,

$$S(t) = Ae^{-t/\tau_e}\int_{-\infty}^{\infty} e^{-([x-x(t)]/\delta_t(t))^2} e^{-([x-xc]/\delta_x)^2} dx$$

$$= \frac{A}{\sqrt{\pi\Delta}} e^{t/\tau_e} e^{-((x(t)-x_c)/\Delta)^2}, \quad \text{where} \quad \Delta = \delta_t^2(t) + \delta_x^2, \tag{2}$$

with the trajectory of the molecular bond, $x=r-r_e$, given as a damped oscillator,

$$x(t) = x_0 e^{-\gamma t} \cos\left(\frac{2\pi}{\tau(t)}\right). \tag{3}$$

This fitting scheme allows the assessment of contributions of electronic population decay, τ_e, time dependent spread of the packet $\delta_t(t)$, vibrational relaxation rate γ that allows for the packet to fall out of the detection window, and a time dependent period of the oscillator $\tau(t)$ taken from the fit to the experimental data [Eq. (1)]. The finite pulse width of the laser is taken into account by convoluting Eq. (2) with a Gaussian of FWHM=90 fs. As shown in Fig. 4 (dash-dot line), the procedure reproduces the signal with good fidelity. The exception is the amplitude of the first peak, which is two times larger in the experiment, which was argued above to be the effect of predissociation. The reproduction assumes a fixed packet width—the packet retains its coherence without any evidence of anharmonic dispersion or dephasing—and requires $\gamma=0$, implying that the decay of the signal amplitude is entirely due to predissociation of the electronic population with time constant $\tau_e=1$ ps; the detection window is wide, $\delta x/x_0=0.3$, and situated on the attractive side of the potential.

DISCUSSION

The absorption spectrum of iodine in ice is nearly identical to that of iodine in water. It would seem that the disorder of the liquid is frozen out in the quench-condensed ice at 128 K. The variation in the observed signal in different parts of the same sample, and the direct observation of grain motion would suggest photothermally driven annealing and the establishment of ordered domains at least in the irradiated parts of the sample. The doped molecule can be expected to trap in a variety of sites, from strictly amorphous to crystalline domains and at grain boundaries. The fact that in such an inhomogeneous sample we should observe coherent vibrational dynamics is noteworthy. The variation between observing X state CARS versus B state TG in different parts of the same sample would indicate a significant variation in the separation between X and B states in different trapping sites. Indeed, the successive 1500 cm^{-1} shift between the free molecule versus clathrate hydrate, and then again between clathrate and ice, indicates the same. In effect, we are selectively observing two identifiable ensembles. The observation of exclusively X-state CARS in certain regions is consistent with selecting molecules trapped in amorphous ice (frozen water), where the shift in electronic origin precludes access of the B-state. In this ensemble, the molecular vibrational frequency is reduced by 6.4%, an effect that is explained in terms of the polarization of the molecule by the local electric field, and therefore trapping in a highly asymmetric site with at least one water molecule oxygen bonded to iodine. The observation of exclusively B-state dynamics in other regions suggests the selective interrogation of an ensemble in which the B state is accessible at 512 nm; moreover, based on the rate of predissociation, it is clear that the molecules in this case are isolated in highly symmetric cages. Both of these observations indicate that the B-state coherence is due to molecules trapped in a clathrate-type structure, where the water molecules of the cage are hydrogen bonded and unavailable to donate an electron pair to iodine. This assignment is further bolstered on energetic grounds, as we expand below in modeling the strongly chirped vibrational coherence in these sites.

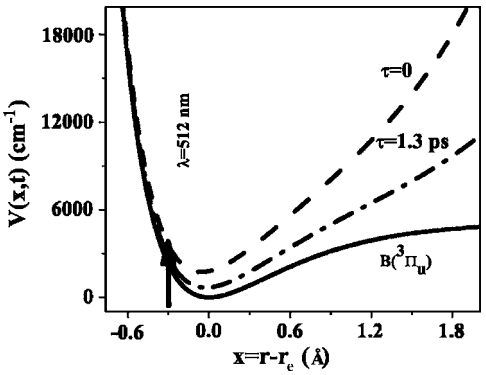

FIG. 6. Time dependent effective potential of I_2 enclathrated in ice. (a) Morse potential of free I_2, effective potential at $t=0$ and $t=1.3$ ps with the exponentially repulsive cage potential. Cage diameter: $d(0)=9.8$ Å and $d(1.3\ \text{ps})=10.68$ Å.

At 512 nm, in the free molecule, $v=39$ of the B state would be prepared, where the period of vibration is 516 fs. Instead, we observe an initial period of 245±20 fs with a spread reflecting site-to-site variation. If we were to assume that the electronic origin of the B state is shifted by ~3500 cm^{-1}, as seen in the absorption spectrum, then the excitation would reach the very bottom of the B potential, where the free molecule period is $1/c\omega_{10}=268.5$ fs. This would seem plausible, until we consider the observed terminal period of vibration of 325±20 fs, which would now correspond to reaching $v=14$. It is not likely that we are observing vibrational up-pumping. There could not be a physical model that explains the period elongation if the initial preparation is at the bottom of the potential. If we were to assume that the observed molecules are trapped in a clathrate-type structure, then the blueshift of 1500 cm^{-1} would prepare the molecule near $v=28$ where the free molecule period is 410 fs. The much shorter observed initial period would have to be ascribed to the molecule being constrained in a tight cage, with the subsequent period elongation to be associated with cage relaxation. We consider a model that is constrained to account for both spectral shift of the transition and the observed periods.

We assume that the molecule is initially in a cage of time dependent diameter $d(t)$ with an exponentially repulsive potential between cage wall and I atoms (Fig. 6). The effective potential experienced by the molecule is

$$V(r,d) = V_{\mathrm{I-I}}(r) + V_{\mathrm{cage}}(r,d) = V_{\mathrm{I-I}}(r) + Ae^{-\alpha[d(t)-r]/2}, \quad (4)$$

in which the first term is the Morse potential of $I_2(B)$, and the time dependence of the cage diameter is taken as the observed chirp, $d(t)=d_0+\delta(1-e^{-t/\tau})$. For the reasonable estimate of $d_0=9.8$ Å, given by the sum of the $I_2(B)$ equilibrium bond length (3.024 Å) and the van der Waals radii of iodine and oxygen atoms,[45] the parameters of the exponential potential ($A=9.56\times10^7$ cm^{-1} and $\alpha=1.11$ Å^{-1}) are adjusted to obtain simultaneously a blueshift of $\sim$1500 cm^{-1} and the observed initial period of motion. The trajectory of the Gaussian packet is then obtained by solving the equation of motion,

$$\mu r(t) + \eta r + \frac{\partial V(r,t)}{\partial r} = 0, \quad \text{with initial conditions}$$

$$r(0) = -0.33 \text{ Å}, \quad r(0) = 0. \quad (5)$$

Assuming no dissipation ($\eta=0$), for the assumed cage potential, the cage diameter must expand from its initial value of $d(0)=9.8$ Å to $d(t=1.3\text{ ps})=10.68$ Å to reproduce the chirped signal. Figure 5 makes it clear that at this terminal distance the molecule is still squeezed. Yet the chirp rate is monotonic, there is no evidence of rebound, suggesting deformation that lacks elasticity on this time scale. If so, one would expect the cage to fully release, such that the B state reaches its free molecule parameters. That can be accomplished by now including a nonzero value for the friction constant in Eq. (5). We adjust η such that the observed terminal period of oscillation is realized upon complete relaxation of the cage potential ($d\sim11.25$ Å). The signal can be reproduced equally well with either model. There are interesting differences between the two. For the case $\eta=0$, the molecule is prepared in $v=10$ of the effective potential, it loses $\sim$250 cm^{-1} of kinetic energy due to cage deformation, and reaches $v=14$ in the terminal potential. While for the case of full relaxation, the molecule loses $\sim$800 cm^{-1} of kinetic energy and remains in $v=10$ throughout. The second model corresponds to the vibrationally adiabatic limit, which is more realistic than the assumption of no dissipation. The analysis suggests fully coherent vibrationally adiabatic following of the cage coordinate.

Note, although the cage does not show any elasticity on the time scale of 2 ps, it must return to its compressed geometry between pulses, in time less than 1 ms. The monotonic dilation of the cage by $\sim$1.4 Å on a time scale of 1.3 ps, without eliciting any rebound, indicates a soft lattice mode of heavy mass, for which a frequency less than 6 cm^{-1} can be estimated. This suggests a cage assembled around the guest molecule in a glassy solid, which based on the preparation conditions is expected to be low-density amorphous ice. The fact that the confining cage mode is soft, nevertheless the molecule is strongly caged such that the effective spring constant it experiences initially is $\sim$50% stiffer, could be understood if the low frequency of the mode is determined by its heavy effective mass (and small spring constant).

CONCLUSIONS

The dynamical investigations of iodine trapped in what is nominally a low-density amorphous ice, along with spectroscopic UV-Vis and Raman measurements previously reported, allow for deeper insights in the nature of the guest molecules trapped in ice. The measurements clearly identify two main ensembles. The first, which we associate with amorphous ice, consists of asymmetric trap sites in which the molecule is strongly polarized through oxygen bonding to one water molecule, with the spectroscopic signatures of a reduced vibrational frequency by 6.4% and a dramatic blueshift of 3500 cm^{-1} in the valence band transitions. The solid, in which this site is exclusively observed, is structurally unstable at the deposition temperature of 128 K, but the instability can be eliminated by annealing at 155 K. Moreover, the only B-state signal observed in this site shows complete predissociation after one extension of the bond. We offer a simple analysis of the vibrational downshift in terms of bond ionicity, to conclude that the molecule must be in a highly polar cage—oxygen bonded on one end and hydrogen bonded on the other. The second site is associated with glassy amorphous ice in which the molecule is trapped in highly symmetric clathrate-type cages, where the molecular vibrational frequency is unperturbed, and the UV-Vis spectrum is blueshifted by 1500 cm^{-1} as in the previously prepared mixed clathrates. Consistent with the concept of symmetry induced electronic caging, we observe the B state to predissociate in 1 ps, only a factor of 2 faster than in cryogenic rare gas solids. The remarkable observation in this site is that vibrational coherences prepared on the excited B state undergo a dramatic period elongation, without losing coherence and with negligible dissipation. The effect is associated with vibrationally adiabatic following of the confining cage coordinate, which undergoes dilation without feedback into the molecule.

ACKNOWLEDGMENTS

This work was supported by the U.S. National Science Foundation (Grant No. CHE-0404743). The authors thank Professors N. Schwentner, P. Devlin, W. Kuhs, and K.C. Janda and Dr. G. Kerenskaya for helpful discussions.

[1] I. Goldschleger, V. Senekerimyan, M. S. Krage, H. Seferyan, K. C. Janda, and V. A. Apkarian, J. Chem. Phys. **124**, 204507 (2006).
[2] G. Kerenskaya, I. U. Goldschleger, V. A. Apkarian, and K. C. Janda, J. Phys. Chem. A **110**, 13792 (2006).
[3] G. Kerenskaya, I. U. Goldschleger, V. A. Apkarian, E. Fleischer, and K. C. Janda, J. Phys. Chem. A **111**, 10969 (2007).
[4] A. C. Legon, J. M. A. Thumwood, and E. R. Waclawik, Chem.-Eur. J. **8**, 940 (2002).
[5] J. B. Davey, A. C. Legon, and J. M. A. Thumwood, J. Chem. Phys. **114**, 6190 (2000).
[6] R. Hernández-Lamoneda, V. Hugo, U. Rosas, M. I. Bernal Uruchurtu, and K. C. Janda, "Two-dimensional H_2O-Cl_2 and H_2O-Br_2 potential surfaces: An *ab initio* study of ground and valence excited electronic states," J. Phys. Chem. A (to be published).
[7] I. Golsdchleger, G. Kerenskaya, K. C. Janda, and V. A. Apkarian, "Polymorphism in Br_2 clathrate hydrates," J. Phys. Chem. A (to be published).
[8] S. A. Corcelli, C. P. Lawrence, and J. L. Skinner, J. Chem. Phys. **120**, 8107 (2004).
[9] I. Goldschleger, V. Senekerimyan, and V. A. Apkarian (unpublished).
[10] F. Pauer, J. Kipfstuhl, W. F. Kuhs, and H. Shoji, J. Glaciol. **45**, 149

(1999).
[11] R. Zadoyan, Z. Li, C. Martens, P. Ashjian, and V. A. Apkarian, Chem. Phys. Lett. **218**, 504 (1994).
[12] N. Schwentner and V. A. Apkarian, Chem. Rev. (Washington, D.C.) **99**, 1481 (1999).
[13] M. Guhr, M. Bargheer, and N. Schwentner, Phys. Rev. Lett. **91**, 085504 (2003).
[14] Z. Bihary, R. Zadoyan, M. Karavitis, and V. A. Apkarian, J. Chem. Phys. **120**, 7576 (2004).
[15] M. Fushitani, N. Schwentner, M. Schroder, and O. Kuhn, J. Chem. Phys. **124**, 024505 (2006).
[16] M. Guhr and N. Schwentner, Phys. Chem. Chem. Phys. **7**, 60 (2005).
[17] M. Bargheer, P. Dietrich, K. Donovan, and N. Schwentner, J. Chem. Phys. **111**, 8556 (1999).
[18] J. Helbing and M. Chergui, J. Chem. Phys. **115**, 6158 (2001).
[19] M. Karavitis and V. A. Apkarian, J. Phys. Chem. B **106**, 8466 (2002).
[20] M. Karavitis, D. Segale, Z. Bihary, M. Pettersson, and V. A. Apkarian, Low Temp. Phys. **29**, 814 (2003).
[21] M. Karavitis, R. Zadoyan, and V. A. Apkarian, J. Chem. Phys. **114**, 4131 (2001).
[22] T. Kiviniemi, J. Aumanen, P. Myllyperkio, V. A. Apkarian, and M. Pettersson, J. Chem. Phys. **123**, 064509 (2005).
[23] R. F. Barrow and K. K. Yee, J. Chem. Soc., Faraday Trans. 2 **69**, 684 (1973).
[24] W. Kiefer and H. J. Bernstein, J. Mol. Spectrosc. **43**, 366 (1972).
[25] E. F. Burton and W. F. Oliver, Nature (London) **135**, 505 (1935).
[26] C. A. Angell, Science **267**, 1924 (1995).
[27] G. P. Johari, A. Hallbrucker, and E. Mayer, Science **273**, 90 (1996).
[28] P. Jenniskens and D. F. Blake, Astrophys. J. **473**, 1104 (1996).
[29] W. Ostwald, Z. Phys. Chem., Stoechiom. Verwandtschaftsl. **34**, 495 (1900).
[30] S. Reiss and K. Heinig, Nucl. Instrum. Methods Phys. Res. B **102**, 256 (1995).
[31] W. Kiefer and H. J. Bernstein, J. Raman Spectrosc. **1**, 417 (1973).
[32] W. Kiefer, Appl. Spectrosc. **28**, 115 (1973).
[33] J. P. Kettle and A. H. Price, J. Chem. Soc., Faraday Trans. 2 **68**, 1306 (1972).
[34] B. L. Grigorenko, A. V. Nemukhin, and V. A. Apkarian, J. Chem. Phys. **104**, 5510 (1996).
[35] B. L. Grigorenko, A. V. Nemukhin, and V. A. Apkarian, Chem. Phys. **219**, 161 (1997).
[36] B. L. Grigorenko, A. V. Nemukhin, and V. A. Apkarian, J. Chem. Phys. **108**, 4413 (1998).
[37] M. Ovchinnikov and V. A. Apkarian, J. Chem. Phys. **110**, 9842 (1999).
[38] B. L. Grigorenko, A. V. Nemukhin, and V. A. Apkarian, Chem. Phys. **232**, 321 (1998).
[39] J. C. D. Brand and A. R. Hoy, Appl. Spectrosc. Rev. **23**, 285 (1987).
[40] F. Ramondo, J. R. Sodeau, T. B. Roddis, and N. A. Williams, Phys. Chem. Chem. Phys. **2**, 2309 (2000).
[41] For an early review, see A. L. Harris, J. K. Brown, and C. B. Harris, Annu. Rev. Phys. Chem. **39**, 341 (1988).
[42] V. S. Batista and D. F. Coker, J. Chem. Phys. **105**, 4033 (1996); **106**, 7102 (1997).
[43] N. F. Scherer, D. M. Jonas, and G. R. Fleming, J. Chem. Phys. **99**, 153 (1993).
[44] R. Zadoyan, M. Sterling, M. Ovchinnikov, and V. A. Apkarian, J. Chem. Phys. **107**, 8446 (1997).
[45] A. Bondi, J. Phys. Chem. **68**, 441 (1964).